ELSEVIER

Colloids and Surfaces A: Physicochem. Eng. Aspects 263 (2005) 129–145

COLLOIDS AND SURFACES A

www.elsevier.com/locate/colsurfa

Wall slip and viscous dissipation in sheared foams: Effect of surface mobility

Nikolai D. Denkov *, Vivek Subramanian, Daniel Gurovich, Alex Lips

Unilever Research & Development, 45 River Road, Edgewater, NJ 07020, USA

Received 23 January 2005; accepted 17 February 2005
Available online 23 May 2005

This article is dedicated to the memory of Dr. Henry Princen, who was one of the pioneers and made eminent contributions in the area of foam and emulsion rheology.

Abstract

Wall-slip is a general phenomenon in the rheological behavior of foams and has to be considered explicitly in the description of foam flow through pipes and orifices, upon spreading on surfaces, and in the rheological measurements. On the other hand, the wall-slip, occurring between a plug of foam and smooth wall, is an appropriate phenomenon for experimental and theoretical study of the viscous friction in liquid films, because the corresponding viscous stress, which is amenable to experimental measurement, does not interfere with the foam elastic stress. The current paper presents a theoretical model and experimental results about the viscous friction between foam and smooth wall. First, the lubrication model is used to calculate the friction force between a single bubble and the wall, in the case of bubbles with tangentially immobile surfaces. Next, the functions introduced by Princen and Kiss [H.M. Princen, A.D. Kiss, Langmuir 3 (1987) 36] to relate the micro-structure of the foam (bubble and film radii, bubble capillary pressure) with the foam macroscopic properties (air volume fraction and foam osmotic pressure) are used to estimate the average, experimentally accessible wall stress, τ_W, from the friction force of individual bubbles. The model predicts $\tau_W \propto (Ca^*)^{1/2}$ where $Ca^* = (\mu V_0/\sigma)$ is the capillary number, defined with respect to the relative velocity of the foam and wall, V_0 (μ is the liquid viscosity and σ the surface tension). This prediction differs from the classical result, $\tau_W \propto (Ca^*)^{2/3}$, derived by Bretherton [F.P. Bretherton, J. Fluid Mech. 10 (1961) 166]. The analysis shows that the two theoretical models correspond to two limiting cases, governed mainly by the surface mobility of the bubbles. These limiting cases are verified experimentally by measuring the viscous stress in the foam/wall region with properly chosen surfactant solutions, which ensure tangentially mobile or immobile surface of the bubbles. Furthermore, it is shown experimentally that the effect of bubble surface mobility affects strongly the viscous friction inside sheared foams. The viscous stress in continuously sheared foam is described very well with a power law, $\tau_V \propto Ca^n$, where Ca is the capillary number defined here with respect to the shear rate inside the foam. The power index n was determined experimentally to be equal to 0.25 ± 0.02 for tangentially immobile and to 0.42 ± 0.02 for tangentially mobile bubble surfaces, respectively, at air volume fraction of 90%.

Keywords: Foam rheology; Foam viscosity; Wall slip; Viscous friction in foams

1. Introduction

The mechanical and rheological properties of foams and concentrated emulsions are important for their applications and attracted the scientific interest in several research areas, including colloid science, soft-matter physics, and materials science [1–19]. During stress-induced deformation and flow of foam or emulsion, the constituent bubbles or drops deform, which causes expansions and contractions of the bubble/drop surfaces [1–13]. As a result, the related capillary phenomena are very important for the rheological properties of foams and emulsions, which usually behave as visco-elastic fluids, with yield stress, even when the constituent phases are Newto-

* Corresponding author at: Laboratory of Chemical Physics and Engineering, Faculty of Chemistry, Sofia University, 1 James Bourchier Ave., 1164 Sofia, Bulgaria. Tel.: +359 2 962 5310; fax: +359 2 962 5643.
E-mail address: nd@lcpe.uni-sofia.bg (N.D. Denkov).

0927-7757/$ – see front matter © 2005 Elsevier B.V. All rights reserved.
doi:10.1016/j.colsurfa.2005.02.038

nian fluids. To find the relation between the micro-structural properties of foams and emulsions (such as bubble/drop size, volume fraction of the dispersed phase, surface forces acting between the dispersed entities), and the macroscopic rheological properties of these systems, is a challenging scientific problem, which has not been fully resolved. A comprehensive review of the current understanding of the rheological properties of foams and concentrated emulsions can be found in Refs. [6,7].

In the present study, we are interested mainly in the rheological properties of foams, which are subject to continuous shear deformation. Theoretical and experimental studies revealed that the foam shear stress, τ, consists of two parts [5–7]:

$$\tau = \tau_0 + \tau_V(\dot{\gamma}) \tag{1.1}$$

where τ_0 is the rate-independent component (called 'elastic stress' or 'yield stress' in literature), τ_V the rate-dependent component, and $\dot{\gamma}$ the rate of shear deformation. The elastic term was found to depend primarily on the mean volume–surface radius of the bubbles, R_{32}, air volume fraction, Φ, and surface tension, σ. The viscous stress, τ_V, depends on the same factors, as well as on the viscosity of the continuous phase, μ, and on the rheological properties of the surfactant adsorption layers [6,7,20–22].

In many cases, the rheological properties of foams and concentrated emulsions were described adequately with the Herschel–Bulkley model [6–15]

$$\tau = \tau_0 + k_V\dot{\gamma}^n \tag{1.2}$$

where n is a power law index and k_V the foam consistency. The index n depends on the specific mechanism of viscous dissipation during the foam flow. By considering uni-axial periodic deformation with small amplitude, and assuming that the viscous dissipation occurs only at the periphery of the films, formed between two adjacent drops/bubbles (i.e., that the central areas of the films remain undisturbed by the deformation), Schwartz and Princen [23] and Reinelt and Kraynik [11] found theoretically that the power index for such type of deformation should be $n = 2/3$. To derive this result, the authors [11,23] modified the theoretical approach of Bretherton [24], which was originally developed to describe the viscous friction between a bubble and solid wall.

The model, developed in Refs. [11,23] for small oscillatory deformations of foams and emulsions, is not directly applicable to the case of continuous shear flow, because the dynamics of film formation and thinning, and the respective viscous dissipation, are rather different in the periodic and continuous modes of foam deformation. For example, the central zone of the liquid films cannot be considered as non-disturbed in the regime of continuous flow, whereas this is an essential assumption in the models describing small deformations [11,23]. Indeed, in a careful experimental study of the viscous dissipation in continuously sheared emulsions, Princen and Kiss [5] found $n \approx 1/2$, which differs from the theoretical prediction $n = 2/3$ [11,23]. Thus, a theoretical model for the viscous dissipation in continuously sheared foams and concentrated emulsions is still missing. One of the major difficulties in the development of such models is the lack of understanding about the role of the surface rheological properties (such as surface elasticity and viscosity of the surfactant adsorption layer), on the macroscopic rheological properties of foams and emulsions. Although some experimental results were presented recently [17,25], which reveal an effect of the surface rheological properties on the viscous dissipation in foams, this relation is far from being understood and described in quantitative terms. On the other hand, the surface properties were found to be very important for another dynamic process in foams, viz. the drainage of liquid from the foam [26–33].

The continuous flow of foams and concentrated emulsion is usually affected by the wall-slip phenomenon, which is rather general in these systems, because: (1) the bubbles and drops are larger than the typical dimensions of the wall corrugations, and (2) the bubbles and drops are deformable, which allows them to surpass these corrugations. For these reasons, usually, the wall slip should be explicitly taken into account in the description of the foam/emulsion flow and in the analysis of rheological data, obtained with such systems [2,5–7,34–36]. On the other hand, the wall-slip, occurring between a plug of foam and smooth wall, is a very appropriate phenomenon for experimental and theoretical study of the effect of surface rheological properties on the viscous friction in liquid films (see Sections 2 and 3 below).

The current study is aimed to test theoretically and experimentally how important are the surface properties of the bubbles for the viscous dissipation inside liquid films, which are formed between bubbles and solid wall (i.e., for the foam–wall friction), as well as between two adjacent bubbles in continuously sheared foam.

To achieve our goal, first, we consider theoretically the viscous friction between a bubble with tangentially immobile surface and smooth solid wall. In the current model we assume that the viscous friction is distributed in the entire area of the wetting film, formed between the bubble and the wall. From this viewpoint, this model differs essentially from the Bretherton's model [24], which assumes that always a certain central portion of the film remains immobile with respect to the wall and, hence, the viscous friction is localized in the front and rear regions of the wetting film (see Section 2.6 below for further discussion of the two models). The model developed in the current study predicts that the wall stress $\tau_W \propto {V_0}^{1/2}$, which is in contrast with the result from the Bretherton's model, $\tau_W \propto {V_0}^{2/3}$, where V_0 is the relative velocity of the bubble and the wall. As explained in Section 2.6, these theoretical models describe two limiting cases for bubbles with tangentially immobile and tangentially mobile surfaces, respectively.

Second, we verify these theoretical predictions by direct measurement of the foam–wall friction stress for foams, prepared with several surfactant solutions, which ensure differ-

ent surface mobility of the bubbles. In agreement with the theoretical models, we measured $\tau_W \propto V_0^{1/2}$ and $\tau_W \propto V_0^{2/3}$ for systems with tangentially immobile and mobile bubble surfaces, respectively. As discussed briefly in Section 2.6, the theoretical analysis and the experimental results for the foam–wall friction, presented in the current study, may be related to another research problem, namely, the motion of bubbles and drops in narrow capillaries [7,24,37–42].

Third, we show experimentally that the surface mobility of the bubbles plays an important role for the viscous friction inside sheared foams — the viscous stress is higher, while the power index n is lower, for bubbles with tangentially immobile surfaces, at equivalent all other conditions. The experimental results show also that the power index for foams is lower ($n \approx 0.25$ for immobile and $n \approx 0.42$ for mobile bubble surfaces, at air volume fraction of 0.90), in comparison with the indexes reported in literature for concentrated emulsions ($0.5 \leq n \leq 0.9$).

The paper is organized as follows: Section 2 describes the theoretical model of the foam–wall friction in the case of tangentially immobile bubble surface. Section 3 presents the main experimental results, and Section 4 summarizes the conclusions.

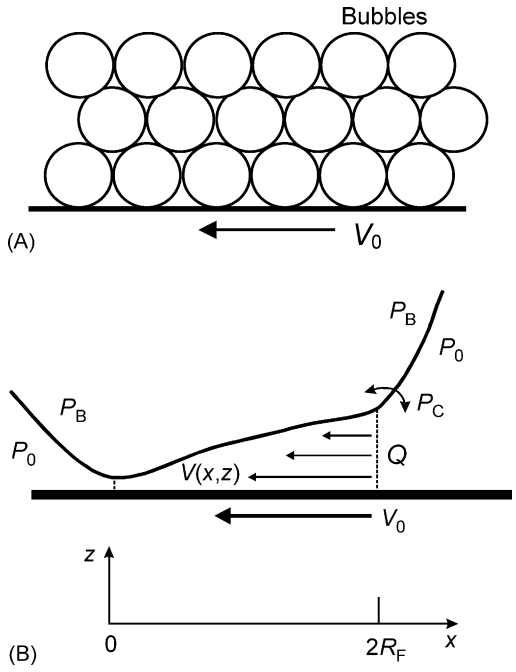

Fig. 1. Schematic presentation of the system under consideration. (A) Smooth solid substrate is moving with constant linear velocity, V_0, with respect to a plug of foam bubbles. (B) The liquid entrainment into the wetting film, formed between the bubble and the moving substrate, leads to an asymmetric film configuration, with larger film thickness in the entrance (front) region.

2. Theoretical model for the viscous friction between a bubble with tangentially immobile surface and smooth solid wall

2.1. Description of the system – used approximations and basic equations

2.1.1. System configuration

We consider the viscous friction between a bubble and solid wall, see Fig. 1. The radius of the wetting film, formed in the zone of bubble–wall contact, is denoted with R_F. The capillary pressure of the bubble is $P_C = (P_B - P_0)$, where P_B is the air pressure inside the bubble and P_0 is the pressure in the aqueous phase around the film (in the Plateau border region). The liquid flow in the actual, three-dimensional (3D) configuration of the system is too complex to allow analytical modeling. For this reason, we make several approximations, which are widely used in the theory of lubrication [43,44] and in the studies on foam structure and rheology [1,6], to make the problem feasible for theoretical analysis.

First, we consider the friction between a two-dimensional (2D), infinitely long cylindrical bubble and a wall (the bubble axis is parallel to the wall). In Section 2.5 below, the expressions derived for the friction force per unit length of such 2D-bubble, are scaled to the case of a 3D-bubble, similar to those in the actual foams, and the respective macroscopic wall stress is calculated for foams consisting of 2D- and 3D-bubbles.

In our consideration, the coordinate system is fixed to the bubble (considered as immobile), while the solid wall slides with a given linear velocity, V_0, in direction perpendicular to the bubble axis (see Fig. 1B). The bubble–wall viscous friction is considered significant only inside the wetting film and in the closest meniscus region (which has a thickness comparable to that of the wetting film), because the viscous stress scales as V_0/h, where h is the local film thickness. Therefore, the contribution to the friction force from the regions, in which the local thickness of the aqueous layer is much greater than the thickness of the wetting film, is negligible.

Under dynamic conditions, the thickness of the wetting film can be 1 to 2 orders of magnitude larger than the equilibrium film thickness, h_{EQ} (typically, 5–30 nm), see Section 2.4 below. The equilibrium film thickness is determined by the surface forces, which are usually expressed in terms of the so-called 'disjoining pressure' (force per unit area of the film) [45–47]. Due to the drag of liquid into the film by the moving wall, the film has larger thickness in the front region, as illustrated in Fig. 1B. Such asymmetric film configuration has been observed and described in the studies of lubrication by liquids (e.g., Refs. [43,48]), and it is very important for establishing higher dynamic pressure inside the film, $P(x)$, as compared to the pressure in the surrounding Plateau regions, P_0. Therefore, in general, the dynamic film has to be characterized not only by its thickness (e.g., the average film thickness, h_{AV}) but also by the slope of its upper surface. Further discussion of the film thickness and shape under equilibrium and dynamic conditions is given in Sections 2.1.5 and 2.4 below.

2.1.2. Lubrication approximation

The hydrodynamic problem for the viscous friction inside the film is solved in the lubrication approximation [43,44]. The latter is justified in most cases of practical interest, because the film thickness is typically several orders of magnitude smaller than the film radius, $h/R_F \ll 1$, the slope of the film surface is small everywhere, $dh/dx \ll 1$, and the Reynolds number, $Re = (h\rho V_0)/\mu \ll 1$, is low ($Re$ is defined with respect to the film thickness and ρ the liquid mass density). Therefore, the liquid flow in the film is adequately described by the lubrication equation [24,43,49]

$$\frac{dP}{dx} = \mu \frac{\partial^2 V_x}{\partial z^2} \tag{2.1}$$

where $P(x)$ is the local pressure in the liquid film. In the lubrication approximation, the pressure depends only on the lateral co-ordinate x and is independent of the vertical co-ordinate z, see Fig. 1B. The lateral component of the fluid velocity, $V_x(x, z)$, is a function of both coordinates, x and z.

Due to the assumed 2D-configuration of the bubble, no dependence on y-coordinate is allowed for any of the studied quantities. Note that all intensive quantities (including the friction force) are defined per unit length of the bubble.

2.1.3. Boundary conditions for the liquid velocity

In general, the surface of the bubble can be tangentially mobile, which implies that a certain surface velocity, $u(x)$, would appear as a boundary condition for solving Eq. (2.1). The function $u(x)$ is unknown in advance and should be found as part of the solution [49,50]. Therefore, the boundary conditions for the fluid velocity at the upper and lower surfaces of the wetting film are

$$V_x(z = 0) = -V_0 \quad V_x(z = h) = -u(x) \tag{2.2}$$

which are defined in such a way that the sliding velocity of the wall, V_0, and the surface velocity, $u(x)$, have positive values (see Fig. 1B). In the following, we consider tangentially immobile bubble surface, that is we assume $u(x) = 0$ everywhere on the upper film surface. The general case of surfaces with partial tangential mobility will be considered in a separate study [51], because it requires an elaborate analysis of the contributions of the surface elasticity and viscosity to the surface stress balance.

2.1.4. Boundary conditions for the pressure

The following boundary conditions for the pressure are used (see Fig. 1B):

$$P(x = 0) = P_0 \quad (a) \qquad P(x = 2R_F) = P_0 \quad (b) \tag{2.3}$$

which account for the fact that the pressure, in the Plateau border regions, is fixed. This assumption is justified by the facts that: (1) the gradient of the fluid velocity in the Plateau borders is small, which means that the viscous stress and the respective dynamic pressure are negligible there, as compared to the viscous stress in the films; (2) the Plateau borders in the actual 3D foam are interconnected, so that the pressure is equilibrated on both sides of the film.

2.1.5. Shape of the upper film surface

In general, the shape of the upper film surface has to be found as a part of the overall solution of the problem, by using the following differential equation, which expresses the normal stress balance at the air–water interface [11,23,24]

$$\sigma \frac{d^3 h}{dx^3} = -\frac{dP}{dx} \tag{2.4}$$

It is shown in Section 2.2, that the right-hand side of Eq. (2.4) can be expressed through the local thickness of the film, $h(x)$, and the liquid flux along the film, Q (defined per unit length of the 2D-bubble)

$$Q = \int_0^h dz\, V_x(x, z) \tag{2.5}$$

The following differential equation for $h(x)$ is derived (see Eq. (2.15) below)

$$\sigma \frac{d^3 h}{dx^3} = 6\mu V_0 \left[\frac{2Q}{V_0 h(x)^3} + \frac{1}{h(x)^2} \right] \tag{2.6}$$

which has no analytical solution. Although a numerical solution of the complete set of equations, including Eq. (2.6), is possible, this requires significant computational efforts. However, the functional dependence of the friction force on the various governing parameters can be derived without such complicated calculations, as explained below, at the expense of the appearance of an unknown numerical constant of the order of unity. Since we are interested in the application of the model to real 3D-systems, the exact value of the constant in the current 2D-model is not of significant interest, because it is lost anyway in the used scaling procedure from the 2D to the 3D-system.

To avoid the cumbersome numerical procedures, which would involve the solution of Eq. (2.6), we use the simplifying assumption that the upper film surface has a certain predescribed shape [43,44,52,53]. This shape is described by two parameters, characterizing the film thickness and slope (see the next paragraph for precise definitions), which are found as part of the overall solution of the problem. Such an approximation for the shape of the film surfaces has been widely used in the lubrication studies [43,44], because it simplifies considerably the computational procedures, at the expense of an uncertainty (often inessential) in the numerical factor multiplying the functional dependence of the friction force on the various parameters involved.

To check how sensitive are the final results to the particular choice of the shape of the upper film surface, we tested two alternative functions to describe the surface profile (see Fig. 2):

Linear profile of the upper film surface

$$h(x) = h_0 + kx \quad \text{linear profile} \tag{2.7}$$

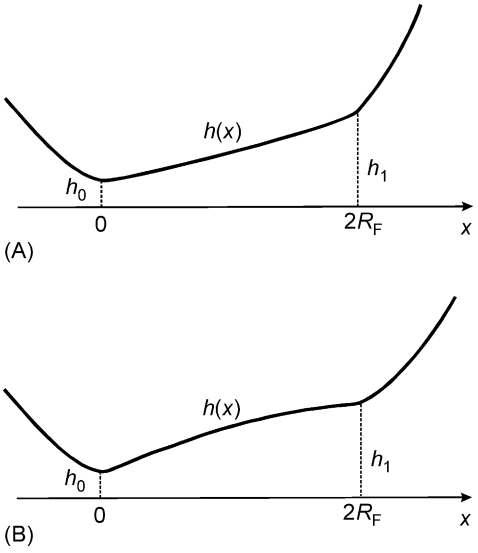

Fig. 2. Schematic presentation of the assumed model profiles of the upper surface of the wetting film: (A) linear profile, Eq. (2.7); (B) curved profile, Eq. (2.8).

Parabolic profile of the upper film surface

$$h(x) = (h_0^2 + 2kx)^{1/2} \quad \text{curved profile} \tag{2.8}$$

In Eqs. (2.7) and (2.8), h_0 is the minimal thickness at the film exit (rear edge of the film), whereas the constant k characterizes the surface slope in the case of linear profile of the film surface, Eq. (2.7), and the surface curvature in the case of curved profile, Eq. (2.8). Note that k has different dimensions in Eqs. (2.7) and (2.8).

The linear profile, Eq. (2.7), was chosen, because it is the simplest possible function that can be used — a certain slope of the film surface is necessary to have a non-zero dynamic pressure in the film, which counterbalances the capillary pressure of the bubble when the latter slides with respect to the wall [43,44,48,53]. The curved profile, Eq. (2.8), resembles more closely the actual film shape, observed under dynamic conditions [48]. As explained in Section 2.3, the final numerical results, based on Eqs. (2.7) and (2.8), are very similar — the respective numerical constants in the calculated friction force differ by less than 3%, which means that the assumption for a particular shape of the upper film surface does not affect strongly the final result.

2.1.6. Constant liquid flux along the film

The incompressibility of the liquid implies that the hydrodynamic flux, Q, should be conserved along the film

$$Q = \int_0^h \mathrm{d}z\, V_x(x, z) = \text{const.} \tag{2.5'}$$

The flux Q is not known in advance and has to be found as a part of the problem solution.

Note that Eq. (2.5′) is used instead of the more detailed, local equation of liquid incompressibility

$$\frac{\partial V_x}{\partial x} + \frac{\partial V_z}{\partial z} = 0 \tag{2.9}$$

because, by adopting the model profiles for the upper film surface, Eq. (2.7) or (2.8), we do not satisfy locally the Laplace equation of capillarity, Eq. (2.4). As a result, the vertical component of the fluid velocity, $V_z(x, z)$, cannot be found as a part of the overall solution (because no appropriate boundary condition is available at the upper film surface), and Eq. (2.9) cannot be used. Thus, Eq. (2.9) is replaced by Eq. (2.5′), which has a meaning of an integral balance of the liquid flux across the film.

2.1.7. Normal force balance

As explained in the previous paragraph, the use of a model film profile, such as Eq. (2.7) or (2.8), precludes the possibility for making a local pressure balance across the film surface. Instead, an integral balance of the pressure acting across the entire upper film surface is to be used to define a closed set of equations

$$\int_{A_F} P_d(x)\,\mathrm{d}A \equiv \int_{A_F} [P(x) - P_0]\,\mathrm{d}A = P_C A_F - \int_{A_F} \Pi(x)\,\mathrm{d}A \tag{2.10}$$

where the integration is over the entire film area, A_F, and we used the fact that P_C is determined only by the bubble size, surface tension, and air volume fraction in the foam, and does not depend on the local co-ordinates. Eq. (2.10) implies that the dynamic pressure inside the film, $P_d(x) = P(x) - P_0$, which acts on the upper film surface from below (defined as an excess with respect to the pressure in the liquid outside the film, P_0), is counterbalanced by the capillary pressure of the bubble, P_C, and the disjoining pressure, $\Pi(h)$. The disjoining pressure accounts for the surface forces (van der Waals, electrostatic, etc.) acting between the two surfaces of the wetting film [45–47]. Since the slope of the film surfaces is assumed small, the dependence of the disjoining pressure on the lateral co-ordinate, x, comes only from the change in the film thickness along x, i.e. $\Pi(x) \equiv \Pi[x(h)]$.

Two limiting cases of the normal force balance, Eq. (2.10), are worthwhile mentioning. First, in the absence of wall slip, $V_0 = 0$, the dynamic pressure is equal to zero (see, e.g., Eqs. (2.19) and (2.24) below), and the force balance is satisfied by equilibrating the capillary pressure with the disjoining pressure in the film, at the respective equilibrium film thickness, h_{EQ}

$$\Pi(h_{EQ}) = P_C \tag{2.11}$$

Eq. (2.11) can be used to find h_{EQ} if the capillary pressure, P_C, and the functional dependence, $\Pi(h)$, are known.

The second limiting case of interest appears when the film thickness, under dynamic conditions, becomes larger than the

range of the surface forces, that is $h \geq 100$ nm everywhere in the film. In this case, Eq. (2.10) reduces to

$$\int_{A_F} P_d(x)\mathrm{d}A = P_C A_F \tag{2.12}$$

The use of the simpler Eq. (2.12), instead of Eq. (2.10) (when justified), is a significant advantage in the analysis of the model and for its application to real data, because no account for the surface forces is needed. Since in most cases the functional dependence, $\Pi(h)$, is unknown, the complete analysis of the rheological data would be either impossible or rather speculative, if the disjoining pressure has to be explicitly considered. As discussed in Section 2.4, this is the typical case for emulsions (the complete Eq. 2.10 has to be used), whereas the simpler Eq. (2.12) is usually applicable to foams. This qualitative difference between foams and emulsions is related to the, typically, much larger size of the foam bubbles, which results in thicker wetting films under dynamic conditions, as compared to emulsion systems.

2.1.8. Friction force

As usual, the friction force on the solid surface is defined as (see Fig. 1B)

$$F_{FR} = \int_{A_F} \mu \left(\frac{\partial V_x}{\partial z}\right)_{z=0} \mathrm{d}A \tag{2.13}$$

Direct check with the final formulas confirmed that the friction force exerted on the wall, Eq. (2.13), is equal in magnitude and opposite in direction to the friction force acting on the bubble.

2.2. Set of equations to be solved

In this section we reformulate Eqs. (2.1)–(2.13) to define the final set of equations used to calculate the friction force. Double integration of the lubrication equation, Eq. (2.1), along with the boundary conditions, Eq. (2.2), leads to the following expression for the liquid velocity in the film

$$V_x(x,z) = \frac{1}{2\mu}\frac{\mathrm{d}P}{\mathrm{d}x} z(z-h) + V_0\left(\frac{z}{h} - 1\right) \tag{2.14}$$

In the above expression, P and h are unknown functions of x, whereas V_0 is a known constant.

Note that $V_x(x, z)$ is a superposition of two qualitatively different flow fields. The second term in the right-hand-side of Eq. (2.14) describes a linear velocity profile, created by the moving substrate (and related to the non-slip boundary condition at the solid surface, Eq. (2.2)). The direction of this flow is the same as the direction of the substrate motion. In contrast, the first term in Eq. (2.14) describes a quadratic profile (Poiseuille type of flow), created by the higher dynamic pressure in the wetting film, as compared to the pressure in the Plateau borders around the film. Since the dynamic pressure is highest in the central film region (see Eqs. (2.19) and (2.24) below), the Poiseuille flow is directed from the film center to the film periphery. Hence, the Poiseuille flow has the same direction as the linear flow in the rear part of the film, and opposite direction in the front part of the film.

By introducing Eq. (2.14) into Eq. (2.5′), one derives the following equation for $P(x)$

$$\frac{\mathrm{d}P}{\mathrm{d}x} = -6\mu\left[\frac{2Q}{h^3} + \frac{V_0}{h^2}\right] \tag{2.15}$$

which can be integrated to derive the following expression for the dynamic pressure $P_d[h(x)]$ in the wetting film

$$P_d(h) \equiv P(h) - P_0 = -6\mu \int_{h_0}^{h} \left[\frac{2Q}{h^3} + \frac{V_0}{h^2}\right]\left(\frac{\mathrm{d}x}{\mathrm{d}h}\right)\mathrm{d}h \tag{2.16}$$

where Q is still unknown constant. The boundary condition, Eq. (2.3a), was used to derive Eq. (2.16). For convenience, we present hereafter all variables, which depend only on x, as functions of the local film thickness h. Since the functional dependence $h(x)$ is assumed to be known (Eqs. (2.7) or (2.8)), the exchange of the variables h and x is trivial. Note, however, that the parameters k and h_0, which appear in Eqs. (2.7) and (2.8) and define the exact shape of the film profile, are not known in advance and have to be determined in the solution of the overall problem.

The normal force balance, Eq. (2.10), can be written in terms of the film thickness as follows

$$\int_{h_0}^{h_1} P_d\left(\frac{\mathrm{d}x}{\mathrm{d}h}\right)\mathrm{d}h = 2R_F P_C - \int_{h_0}^{h_1} \Pi(h)\left(\frac{\mathrm{d}x}{\mathrm{d}h}\right)\mathrm{d}h \tag{2.17}$$

where h_1 is the thickness of the film entrance (see Fig. 2). Note that h_1 and h_0 are interrelated through Eqs. (2.7) or (2.8). That is, h_1 can be calculated, if h_0 and k are known.

Finally, the friction force, Eq. (2.13), can be rewritten by using Eqs. (2.14) and (2.15) to obtain

$$F_{FR} = (\mu)\int_{h_0}^{h_1}\left[\frac{6Q}{h^2} + \frac{4V_0}{h}\right]\left(\frac{\mathrm{d}x}{\mathrm{d}h}\right)\mathrm{d}h \tag{2.18}$$

The set of Eqs. (2.16)–(2.18) can be further elaborated into a more convenient for analysis and calculations form, if the explicit dependence $x(h)$ is introduced. Since the final set of equations depends on the particular film profile assumed, we present separately the equations for linear and curved film profiles.

2.2.1. Linear film profile

Using Eq. (2.7) to replace the function $x(h)$ in Eq. (2.16), and introducing the dimensionless variable $\xi(x) \equiv h(x)/h_0$, one derives the following equation for the dynamic pressure inside the film

$$P_d(\xi) = 12\mu\left(\frac{V_0 R_F}{h_0^2}\right)\left[1 + \tilde{Q}\frac{(\xi+1)}{\xi}\right]\frac{(1-\xi)}{\xi(\xi_1 - 1)} \tag{2.19}$$

where $\xi_1 \equiv h_1/h_0$ is the dimensionless film thickness at the film entrance, and $\tilde{Q} \equiv Q/(V_0 h_0)$ is the dimensionless liquid

flux along the film. By using the boundary condition, Eq. (2.3b), one derives the following expression for $\tilde{Q}$

$$\tilde{Q} = -\frac{\xi_1}{(\xi_1 + 1)} \tag{2.20}$$

One can substitute Eq. (2.20) into Eq. (2.19) to eliminate $\tilde{Q}$ from the expression for the dynamic pressure

$$P_d(\xi) = 12\mu \left(\frac{V_0 R_F}{h_0^2}\right) \frac{(\xi - 1)}{\xi^2} \frac{(\xi_1 - \xi)}{(\xi_1^2 - 1)} \tag{2.19'}$$

Introducing Eq. (2.19′) into Eq. (2.17), one derives the following relationship between the capillary pressure and the minimal film thickness, h_0, which represents the normal force balance

$$P_C = 12\mu \left(\frac{V_0 R_F}{h_0^2}\right) \frac{\left[\ln \xi_1 - \frac{2(\xi_1 - 1)}{\xi_1 + 1}\right]}{(\xi_1 - 1)^2} + \int_{h_0}^{h_1} \Pi(h) \left(\frac{dx}{dh}\right) \frac{dh}{2R_F} \tag{2.21}$$

Using Eq. (2.20) for $\tilde{Q}$, one can present the friction force in the form

$$F_{FR} = \mu A_F \left(\frac{V_0}{h_0}\right) \frac{\left[4 \ln \xi_1 - \frac{6(\xi_1 - 1)}{\xi_1 + 1}\right]}{\xi_1 - 1} \tag{2.22}$$

Finally, expressing h_0 from Eq. (2.21) (at negligible contribution of the disjoining pressure into the normal force balance, see Section 2.4), and introducing it into Eq. (2.22), one derives the following formula for the friction force

$$F_{FR} = A_F \left(\frac{\mu V_0 P_C}{R_F}\right)^{1/2} \frac{\sqrt{3}\left[\frac{2}{3} \ln \xi_1 - \frac{\xi_1 - 1}{\xi_1 + 1}\right]}{\left[\ln \xi_1 - \frac{2(\xi_1 - 1)}{\xi_1 + 1}\right]^{1/2}} \quad \text{(negligible } \Pi\text{)} \tag{2.23}$$

If the contribution of the disjoining pressure, $\Pi(h)$, cannot be neglected in the normal force balance, Eq. (2.21), then one can again express h_0 from Eq. (2.21) and introduce it into Eq. (2.22) to derive an expression for F_{FR}, which includes $\Pi(h)$.

Note that, in Eqs. (2.19)–(2.23), we expressed in an explicit way the contributions of the dimensional parameters (substrate velocity, V_0, film radius, R_F, film area, A_F, liquid viscosity, μ, and film thickness, h_0), which scale the various quantities. The dimensionless part in these equations depends only on $\xi_1 = h_1/h_0$. Since V_0, R_F, A_F, and μ are assumed to be known quantities, the complete solution of the problem requires one to find h_0 and h_1 (or h_0 and ξ_1).

2.2.2. Curved film profile

By using Eq. (2.8) for the function $x(h)$, and following the steps from Section 2.2.1 above, one derives the following counterparts of Eqs. (2.19)–(2.23)

$$P_d(\xi) = 24\mu \left(\frac{V_0 R_F}{h_0^2}\right) \frac{\left[\frac{\xi_1 \ln \xi_1}{\xi_1 - 1}\left(1 - \frac{1}{\xi}\right) - \ln \xi\right]}{\xi_1^2 - 1} \tag{2.24}$$

$$\tilde{Q} = -\frac{1}{2}\left(\frac{\xi_1 \ln \xi_1}{\xi_1 - 1}\right) \tag{2.25}$$

$$P_C = 12\mu \left(\frac{V_0 R_F}{h_0^2}\right) \frac{[\xi_1^2 - 1 - 2\xi_1 \ln \xi_1]}{(\xi_1^2 - 1)^2} + \int_{h_0}^{h_1} \Pi(h) \left(\frac{dx}{dh}\right) \frac{dh}{2R_F} \tag{2.26}$$

$$F_{FR} = 2\mu A_F \left(\frac{V_0}{h_0}\right) \frac{\left[4(\xi_1 - 1) - 3\frac{\xi_1 \ln^2 \xi_1}{\xi_1 - 1}\right]}{\xi_1^2 - 1} \tag{2.27}$$

$$F_{FR} = A_F \left(\frac{\mu V_0 P_C}{R_F}\right)^{1/2} \frac{\sqrt{3}\left[\frac{4}{3}(\xi_1 - 1) - \frac{\xi_1 \ln^2 \xi_1}{\xi_1 - 1}\right]}{[\xi_1^2 - 1 - 2\xi_1 \ln \xi_1]^{1/2}} \quad \text{(negligible } \Pi\text{)} \tag{2.28}$$

The dimensional multipliers in the above equations are the same as in the case of linear upper film surface (Section 2.2.1). The difference between the two film shapes is reflected only in the dimensionless term expressed through ξ_1.

2.3. Numerical solutions

For illustration, we consider the equation for the friction force in the case of curved film profile, by neglecting the contribution of the disjoining pressure, $\Pi(h)$, in the normal force balance. As explained in Section 2.4 below, $\Pi(h)$ can be neglected for dynamic wetting films between foam bubbles and wall, because these films are typically thicker than the range of surface forces.

In Eqs. (2.24)–(2.28), there is only one unknown quantity, ξ_1, which characterizes the film shape. To find ξ_1, we applied the principle of minimal rate of energy dissipation, which is valid for dynamic systems, which are not far away from thermodynamic equilibrium [54]. According to this principle, at fixed external conditions, a non-equilibrium thermodynamic system will follow a path in the configuration space, which corresponds to minimal rate of energy dissipation.

Applied to our system, this principle implies that the deformable surface of the wetting film (which is the only 'free' internal variable in the system under consideration) would acquire a shape, which ensures minimal rate of energy dissipation. Because the rate of energy dissipation is equal to the work performed by the friction force per unit time, i.e. to $F_{FR}V_0$, this requirement is equivalent to the requirement that the friction force, F_{FR}, is minimal, at fixed all external variables (such as V_0, μ, etc.). Indeed, we found that the function $F_{FR}(\xi_1)$, expressed through Eq. (2.23) or (2.28),

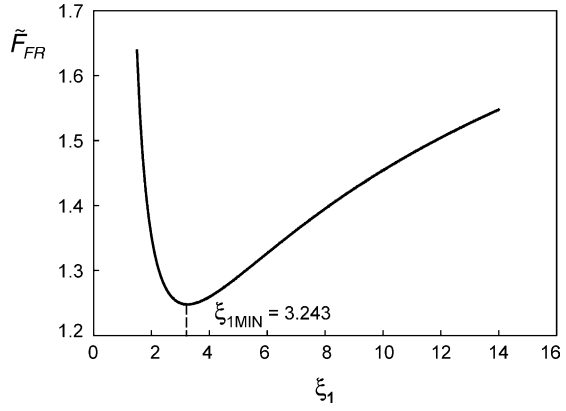

Fig. 3. Plot of the dimensionless friction force, $\tilde{F}_{FR} = (F_{FR}/A_F)(R_F/\mu V_0 P_C)^{1/2}$, as a function of the slope of the upper film surface for curved profile of the film, Eq. (2.28). The minimum in the curve corresponds to minimal rate of energy dissipation in the wetting film.

has a well defined minimum at a certain value $\xi_{1MIN} \approx 3$, see Fig. 3. The numerical calculations showed that $\xi_{1MIN} = 3.243$ for curved film profile and $\xi_{1MIN} = 3.072$ for linear film profile. Substituting these values in Eqs. (2.25)–(2.28) and Eqs. (2.20)–(2.23), respectively, one obtains explicit expressions (including the respective numerical constants) for the various quantities, which characterize the dynamic wetting films, see Table 1. The obtained theoretical values of ξ_{1MIN} show that the upper surface of the wetting film is inclined, with $h_1/h_0 \approx 3$ (see Fig. 2), to ensure lowest rate of energy dissipation in the film. According to the model, ξ_{1MIN} should not depend on the specific experimental conditions (V_0, μ, σ, R_0, R_F, and Φ) for bubbles with tangentially immobile surfaces, if the main assumptions of the model are fulfilled.

Table 1 contains also expressions for the average film thickness, h_{AV}, defined as

$$h_{AV} = \frac{1}{2R_F}\int_0^{2R_F} h\,\mathrm{d}x \tag{2.29}$$

For linear profile of the upper film surface $h_{AV} = h_0(\xi_1 + 1)/2$. For curved film profile, the integral in Eq. (2.29) is calculated by using Eq. (2.8).

As seen from Table 1, the difference in the numerical prefactor for the friction force, calculated for the two film shapes, is less than 3% (1.28 for linear profile against 1.25 for curved profile). The differences between the numerical factors for the other quantities are somewhat larger (5–10%), but they cancel each other almost completely, when F_{FR} is calculated. This comparison shows that the particular shape, chosen to describe the upper film surface, has no large impact on the final result for the friction force, at least for tangentially immobile surface of the bubbles.

The model predicts that both h_{AV} and F_{FR} are proportional to $(\mu V_0)^{1/2}$ for tangentially immobile surface. If one expresses the capillary pressure as $P_C \approx \sigma/R_{PB}$, where R_{PB} is the mean radius of curvature of the Plateau border outside the film, one can presents the results for h_{AV} and F_{FR} in terms of the capillary number, $Ca^* = (\mu V_0/\sigma)$. Thus, for linear profile of the upper film surface one obtains

$$\frac{h_{AV}}{R_0} = 1.10\frac{(R_F R_{PB})^{1/2}}{R_0}(Ca^*)^{1/2} \tag{2.30}$$

$$\frac{F_{FR}}{(\sigma A_F)} = \frac{1.28(Ca^*)^{1/2}}{(R_F R_{PB})^{1/2}} \tag{2.31}$$

Note that F_{FR} is defined per unit length of the 2D-bubble. The radius of the non-deformed bubble of the same volume, R_0, was used for scaling of h_{AV} in Eq. (2.30). Further discussion of these results and their relation to the theoretical predictions of the Bretherton's model [24], is presented in Section 2.6 below.

2.4. Numerical estimates of the average film thickness, h_{AV}

The estimates in this section are made for foam consisting of 2D-bubbles. One may expect that the film thickness in the real 3D-foams will be of the same order of magnitude. To estimate h_{AV} in foam systems, one can neglect the disjoining pressure for reasons explained after Eq. (2.32) below. For this estimate one can assume $R_{PB} \approx R_0$ in Eq. (2.30) to obtain

$$\frac{h_{AV}}{R_0} \approx \left(\frac{R_F}{R_0}\right)^{1/2}(Ca^*)^{1/2} \tag{2.32}$$

The ratio of the film to the bubble radius, R_F/R_0, which appears in Eq. (2.32), depends on the air volume fraction, Φ, and is typically in the range between 0.1 and 1. Typical ranges for the parameters in foam systems, used in detergency, are: $\mu \sim 1$–10^3 mPa s, $\sigma \sim 20$–30 mN/m, and $R_0 \sim 100$–1000 μm. If one takes the following values for the

Table 1
Comparison of the numerical results for 2D bubble with tangentially immobile upper film surface having linear or curved profile

Quantity	Linear profile, Eq. (2.7)	Curved profile, Eq. (2.8)
$\xi_{1MIN} = h_1/h_0$	$\xi_{1MIN} = 3.072$	$\xi_{1MIN} = 3.243$
Liquid flux, Q	$Q = -0.754V_0h_0$	$Q = -0.850V_0h_0$
Minimal film thickness, h_0	$h_0 = 0.540\left(\frac{\mu R_F V_0}{P_C}\right)^{1/2}$	$h_0 = 0.500\left(\frac{\mu R_F V_0}{P_C}\right)^{1/2}$
Average film thickness, h_{AV}	$h_{AV} = 2.04h_0 = 1.10\left(\frac{\mu R_F V_0}{P_C}\right)^{1/2}$	$h_{AV} = 2.32h_0 = 1.16\left(\frac{\mu R_F V_0}{P_C}\right)^{1/2}$
Friction force, F_{FR}	$F_{FR} = 0.693\mu A_F\left(\frac{V_0}{h_0}\right) = 1.28A_F\left(\frac{\mu V_0 P_C}{R_F}\right)^{1/2}$	$F_{FR} = 0.624\mu A_F\left(\frac{V_0}{h_0}\right) = 1.25A_F\left(\frac{\mu V_0 P_C}{R_F}\right)^{1/2}$
Average viscous stress in the film	$\langle\tau_F\rangle = 1.28\left(\frac{\mu V_0 P_C}{R_F}\right)^{1/2}$	$\langle\tau_F\rangle = 1.25\left(\frac{\mu V_0 P_C}{R_F}\right)^{1/2}$

The contribution of the disjoining pressure is neglected, which is justified for typical foam systems (see Section 2.4).

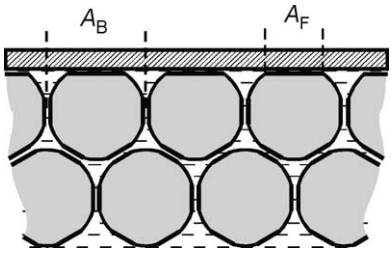

Fig. 4. Schematic presentation of the areas occupied by one bubble, A_B, and by the wetting film, A_F, on the surface of the solid wall.

numerical estimate: $\mu = 1$ mPa s, $\sigma = 20$ mN/m, $R_0 = 50$ μm, $R_F/R_0 = 0.5$, and $V_0 \sim 1$ cm/s, one obtains $Ca^* \sim 5 \times 10^{-4}$ and $h_{AV} \sim 800$ nm.

Note that the estimated film thickness is much larger than the typical range of action of the surface forces. From Eq. (2.32) one can see that this is the case with foam systems, which usually have equal or higher viscosity and larger bubble size, than those used in the above estimate. The film thickness can become comparable to the range of surface forces only under static conditions and at rather low velocities, $V_0 \leq 0.01$ cm/s, or at very low air volume fraction (approaching the one for close-packing of non-deformed bubbles) when $R_F/R_0 \ll 1$.

This estimate of h_{AV} justifies a posteriori our assumption that one can neglect the disjoining pressure in the *wetting films for foam systems under dynamic conditions*. Note, however, that the drop radius in typical *emulsion* systems is much smaller, $R_0 = 3$ μm, which would predict $h_{AV} \sim 50$ nm, that is the surface forces could be important for the wetting films in emulsion systems.

2.5. Estimate of the average wall stress from the friction force of a single bubble

In general, the relation between the wall stress, τ_W, and the friction force per one bubble, F_{FR}, can be expressed through the relation

$$\tau_W = \frac{F_{FR}}{A_B} = \langle \tau_F \rangle f_{2,3}(\Phi) \tag{2.33}$$

where A_B is the average area, occupied by one bubble on the solid wall; $\langle \tau_F \rangle = F_{FR}/A_F$ is the average friction stress in the area of the wetting film, and the function $f_{2,3}(\Phi) \equiv A_F/A_B$ describes the relative area of the solid wall, which is covered by wetting films in 2D- or 3D-foam (denoted by the subscripts 2 and 3, respectively), see Fig. 4.

For a closely packed, regular array of 2D-bubbles, like those considered above, the dependence of the capillary pressure, P_C, A_B and f_2 on the volume fraction of the bubbles was theoretically derived by Princen [1,2]

$$P_C = \left(\frac{\sigma}{R_0}\right)\left[\frac{\Phi(1-\Phi_0)}{\Phi_0(1-\Phi)}\right]^{1/2} \tag{2.34}$$

$$f_2(\Phi) = \left[1 - \left(\frac{1-\Phi}{1-\Phi_0}\right)^{1/2}\right] \tag{2.35}$$

$$A_B = 2R_0\left(\frac{\Phi_0}{\Phi}\right)^{1/2} \tag{2.36}$$

where $\Phi_0 = \pi/2\sqrt{3} \approx 0.91$ is the volume fraction at close-packing of the non-deformed 2D cylindrical bubbles. Combining Eqs. (2.33)–(2.36) with Eq. (2.28) for curved film profile (taking $\xi_{1MIN} = 3.243$, see Table 1) one estimates the following macroscopic, average friction stress on the wall for a 2D-foam

$$\tau_W = 1.25\left(\frac{\mu V_0}{\sigma}\right)^{1/2}\left(\frac{\sigma}{R_0}\right)\left(\frac{\Phi}{\Phi_0}\right)^{1/2} \times \left(\frac{(1-\Phi_0)^{1/2}}{(1-\Phi)^{1/2}} - 1\right)^{1/2} \quad \text{(2D-foam)} \tag{2.37}$$

Equation (2.33) can be used as a starting point to estimate the wall stress in the case of a 3D-foam, as well, if one makes the assumption that the average stress in the wetting film in 3D foam is proportional to the respective average stress in 2D foam. For 3D systems, one should use the functions, found experimentally by Princen and Kiss [3,4,6] to describe typical polydisperse emulsions:

$$f_3(\Phi) \approx 1 - 3.2\left(\frac{\Phi}{1-\Phi} + 7.7\right)^{-1/2} \tag{2.38}$$

$$P_C = \frac{\Pi_{OSM}(\Phi)}{f_3(\Phi)} = \left(\frac{\sigma}{R_{32}}\right)\frac{\tilde{\Pi}_{OSM}(\Phi)}{f_3(\Phi)} \tag{2.39}$$

Here Π_{OSM} is the osmotic pressure of the foam/emulsion and $\tilde{\Pi}_{OSM}$ is its dimensionless counterpart, which is known from the experiments of Princen and Kiss [4]. For a 3D-system

$$A_F = \pi R_F^2 = A_B f_3(\Phi) \tag{2.40}$$

and one can assume also that (see Ref. [55])

$$A_B \approx \pi R_0^2 \tag{2.41}$$

Combining Eqs. (2.38)–(2.41) with Eq. (2.33), one obtains

$$\tau_W = C_{IM}\frac{A_F}{A_B}\left(\frac{\Pi_{OSM}}{f_3}\frac{\mu V_0}{R_F}\right)^{1/2} = C_{IM}F(\Phi)\frac{\sigma}{R_{32}}(Ca^*)^{1/2} \times (\text{3D-foam, tangentially immobile bubble surface}) \tag{2.42}$$

where the dimensionless function $F(\Phi)$ is defined as

$$F(\Phi) \equiv [\tilde{\Pi}(\Phi)]^{1/2}[f_3(\Phi)]^{1/4} \tag{2.43}$$

and it accounts for the dependence of the friction stress on Φ. To find $F(\Phi)$ we used the expression for $\tilde{\Pi}(\Phi)$ which was determined experimentally by Princen and Kiss (see Eqs. (13), (15), and (24) in Ref. [4]). We found that a very good

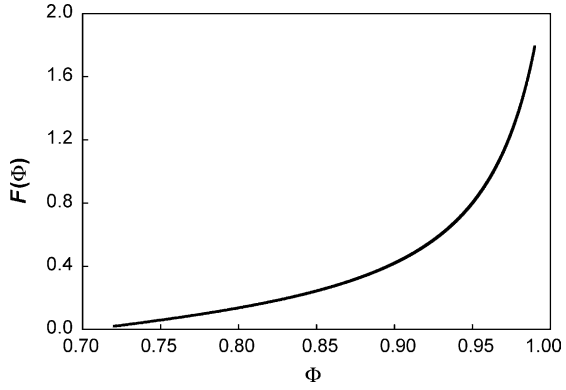

Fig. 5. Graphical presentation of the function $F(\Phi)$, defined by Eqs. (2.43) and (2.44).

numerical approximation of $F(\Phi)$ is given by the following expression (see Fig. 5)

$$F(\Phi) \approx \frac{(0.511 - 0.731\Phi)}{(1 - 5.12\,\Phi + 4.03\,\Phi^2)}, \quad 0.73 < \Phi < 0.99 \tag{2.44}$$

Numerical checks showed that Eq. (2.44) deviates less than 1% from the results, calculated by using the original Princen's functions [4,6], in the entire range of volume fractions of interest, $0.73 < \Phi < 0.99$.

The unknown numerical constant, C_{IM}, in Eq. (2.42) accounts for the fact that the theoretical expression for F_{FR} is derived for a 2D-bubble, whereas it is applied for 3D-foam here. The value of C_{IM} can be found by comparing the predictions of Eq. (2.42) with experimental results (see Section 3.3.1). As a first approximation, one can expect that C_{IM} does not depend on Φ. However, one cannot exclude the possibility that there is some dependence of C_{IM} on Φ, because the assumption that the friction between the bubble and the wall is concentrated only in the wetting film is an approximation. Some friction is expected to occur in the meniscus region surrounding the film, because the viscous stress decays relatively slowly with the film thickness (as h^{-1}). One can expect that, in reality, C_{IM} is a slowly decreasing function of Φ, because the relative effect of the viscous stress, originating from the meniscus region, should decrease with increasing the dimensionless film radius, R_F/R_B (the dimensional analysis predicts that the friction in the meniscus region should scale with R_F, whereas the friction in the film scales with R_F^2).

Starting from the Bretherton result for the friction force (per unit length) of a long 2D-bubble [24]

$$F_{FR} = 4.70\sigma(\mathrm{Ca}^*)^{2/3} \tag{2.45}$$

one can use Eq. (2.33) to derive an estimate for the wall stress in a 3D-foam with tangentially mobile bubble surface. To make this estimate one can assume that the friction in the 3D-wetting film is proportional to the projection of the film periphery along the axis, which is perpendicular to the fluid flux (i.e. proportional to $2R_F$), see Refs. [40,41]. Thus from Eqs. (2.33), (2.40), (2.41) and (2.45) one obtains

$$\tau_W = 3.0C_M \left(\frac{\sigma}{R_{32}}\right) f_3^{1/2}(\Phi)(\mathrm{Ca}^*)^{2/3}$$
tangentially mobile surface (2.46)

where the subscript M in the numerical constant C_M denotes mobile bubble surface.

In conclusion, Eqs. (2.42) and (2.46) are suggested for estimate of the viscous stress due to the wall-slip in real 3D-foams, with tangentially immobile and mobile bubble surfaces, respectively. The numerical constants C_{IM} and C_M are determined in Section 3.3.1 from the comparison of the theoretical predictions with the experimental results.

2.6. Comparison of the current model with Bretherton's model [24]

According to Eq. (2.42), the wall stress $\tau_W \propto (\mathrm{Ca}^*)^{1/2}$, which is in contrast to the prediction of the Bretherton model, $\tau_W \propto (\mathrm{Ca}^*)^{2/3}$. The aim of this section is to explain the reasons for the different predictions of these two models.

The analysis of the assumptions, made in the development of the two models, reveals that the main difference originates from the assumed region, in which the viscous dissipation of energy takes place. In the model developed in Section 2 of this study, the viscous friction is assumed to occur in the entire area of the wetting film. In contrast, Bretherton assumes that there is always a central zone of the wetting film, in which the liquid moves with the velocity of the wall (in a plug flow) and, hence, there is no viscous dissipation in this zone. Thus Bretherton considers a viscous dissipation only in the front and rear edges of the film. Since the viscous dissipation in the front edge is prevailing [24], we will neglect for simplicity, in our further discussion, the dissipation in the rear edge of the film (the conclusions remain unaffected by this simplification).

The main difference between the two models is illustrated in Fig. 6, which shows shaded the energy dissipation zones in the two models. In the current model, the area of the dissipation zone is assumed equal to the entire film area, $A_{FR} = A_F$, independently of the wall velocity and the value of Ca*, whereas A_{FR} in Bretherton's model increases with the velocity of the wall and with the capillary number, $A_{FR} \propto (\mathrm{Ca}^*)^{1/3}$. Furthermore, the different dissipation zones, assumed in the two models, result in different functional dependences of the average film thickness, h_{AV}, on Ca*. In the current model $h_{AV} \propto (\mathrm{Ca}^*)^{1/2}$, see Table 1, whereas $h \propto (\mathrm{Ca}^*)^{2/3}$ in the Bretherton's model (see Eq. (17) in Ref. [24]). Taking into account that the dimensional analysis of the friction force requires

$$F_{FR} = \int_{A_{FR}} \mu \left(\frac{\partial V_x}{\partial z}\right)_{z=0} \mathrm{d}A \approx \mu \left(\frac{V_0}{h_{AV}}\right) A_{FR} = \sigma \mathrm{Ca}^* \left(\frac{A_{FR}}{h_{AV}}\right) \tag{2.47}$$

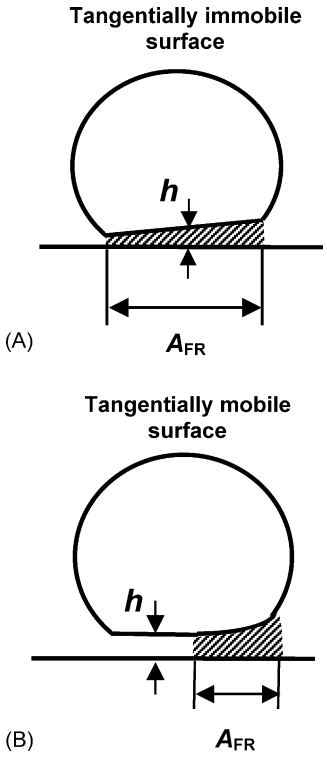

Fig. 6. Schematic presentation of the zones of viscous friction, A_{FR}, in the cases of (A) tangentially immobile bubble surface, and (B) tangentially mobile bubble surface.

one sees that F_{FR} scales with $\sigma(Ca^*)^{1/2}$ in the current model and with $\sigma(Ca^*)^{2/3}$ in the Bretherton's model, due to the different functional dependences of A_{FR} and h_{AV} on Ca^*.

It is worthwhile emphasizing that Bretherton considered two sub-cases in his paper [24]. In the first case (Section 2.1 in Ref. [24]) he assumed that the bubble surface is free from tangential stress everywhere. Obviously, this case corresponds to tangentially mobile bubble surface. In the second case (Section 3.2 in Ref. [24]) he assumed zero tangential velocity, i.e. tangentially immobile surface, in the *front edge* of the bubble. However, in both cases Bretherton assumed that *there is no friction in the central zone of the film*, which would be impossible if the entire surface of the bubble behaves as tangentially immobile — otherwise, the upper surface of the wetting film in its central zone would have different velocity than the wall and viscous friction would occur there. In other words, the second case in Bretherton's analysis assumes that there is a change in the surface mobility of the bubble — the surface is tangentially immobile in the front edge of the bubble, but 'yields' in a transition zone to allow for the bubble surface velocity in the central zone to become equal to the wall velocity. As explained by Bretherton [24], the final results for the two cases, considered by him, differ only in the numerical multiplier, whereas the functional dependence of the friction force on the governing parameters remains the same. The difference in the numerical multipliers, for the two cases considered by Bretherton, was shown theoretically to be no larger than $4^{2/3} \approx 2.52$ [39,42]. In conclusion, one can classify the sub-cases considered by Bretherton as corresponding to tangentially mobile bubble surface (sub-case 1) and to partially tangentially mobile surface (sub-case 2), which are both qualitatively different from the case of tangentially immobile bubble surface (everywhere), considered in Section 2 of the current paper.

Let us note, that numerous experimental studies of the motion of bubbles and drops in thin capillaries [24,37,38,41], aimed to verify Bretherton's model, showed significant deviations from its theoretical predictions. Moreover, it was experimentally established in several studies [38,41,56,57] that the driving pressure pushing a single bubble or a train of bubbles along the capillary (which is related to the friction force in our consideration), as well as the thickness of the wetting film formed between the bubble and the wall of the capillary, scale with $(Ca^*)^{1/2}$. Further theoretical analysis would be helpful to reveal whether these experimental results, puzzling the researchers for many years, could be explained by a model, similar to the one described in the current study.

3. Experimental verification of the theoretical models for the foam–wall viscous stress

In this section, we briefly present experimental results, which clearly show that two qualitatively different cases can be distinguished, depending on the surface dilatational modulus, E_S, of the solutions used for foam generation. Surfactant solutions with high values of E_S exhibit $\tau_W \propto (Ca^*)^{1/2}$, which indicates tangentially immobile surface of the bubbles in these systems. In contrast, the foam–wall friction for foams, generated from solutions with low E_S, scales with $(Ca^*)^{2/3}$, as predicted by Bretherton. It is worthwhile noting that, in the general case, the surface mobility of the bubbles depends on a variety of factors, beside the surface modulus, E_S. The detailed theoretical analysis of the foam–wall friction [51] shows that that the surface mobility depends also on the wall velocity, V_0, liquid viscosity, μ, film radius, R_F, and capillary pressure, P_C. Since the analysis of the effects of all these factors on the bubble surface mobility is beyond the scope of the current study, in the following consideration we will use for simplicity only the surface modulus, E_S, as a characteristic of surface mobility. The latter simplification is justified because both the theoretical analysis [51] and the experimental results presented below evidence that, in our experiments, high values of E_S ensure tangentially immobile bubble surfaces and vice versa.

A detailed description of the experimental procedures and of the obtained results will be presented elsewhere. Here we focus mainly on the comparison of the experimental results with the predictions of the theoretical models and on the role of E_S.

3.1. Experimental methods

3.1.1. Measurement of surface dilatational modulus, E_S

The surface dilatational modulus of the surfactant solutions was measured by the oscillating drop method on FTA4100 instrument (First Ten Ångstroms, USA). The principle of the method is the following: By using a syringe, driven by a motor, small oscillations are generated in the volume of a drop, hanged on a needle tip. These oscillations lead to periodical expansions/contractions of the drop surface with a frequency, ω_0. Video-images of the oscillating drop are recorded and analyzed by means of the Laplace equation of capillarity to determine the surface tension, $\sigma(t)$, and the drop area, $A_D(t)$, as functions of time. To determine the surface dilatational modulus, E_S, which is a measure of the amplitude of surface tension variation due to drop area oscillations, first, the Fourier transforms of $A_D(t)$ and $\sigma(t)$ are calculated to obtain the functions $A_D(\omega)$ and $\sigma(\omega)$, in the frequency domain of surface expansions/contractions. Then, E_S is found as a ratio of the heights of the peaks for $\sigma(\omega)$ and $A_D(\omega)$ at the frequency of the forced oscillations, ω_0.

E_S consists of two components [58,59]

$$E_S = (E_{EL}^2 + E_{LS}^2)^{1/2} \tag{3.1}$$

where E_{EL} is the surface elastic modulus (called also storage modulus), whereas E_{LS} is the loss modulus related to surface dilatational viscosity. In the following consideration we will not discuss the components of E_S, because both high surface elasticity and high surface viscosity suppress the tangential mobility of the surface. More detailed analysis of the role of elastic and viscous components of E_S in the foam–wall friction, will be given elsewhere [51].

In our experiments, the oscillation frequency was fixed at $\omega_0 = 0.785$ rad/s = 0.125 Hz, and the amplitude was between 1 and 3%. The attempts to measure E_S at higher oscillation frequency, with the instrument available, resulted in irreproducible results.

3.1.2. Foam generation and measurement of the mean bubble size

To generate foam with fixed volume fraction of bubbles, $\Phi = 0.9$, we used a 10 mL syringe, equipped by a stainless steel needle with internal diameter of 2.5 mm (Hamilton, Cat. no. 7730-05). First, 1 mL of the surfactant solution was sucked into the syringe. Afterwards, 0.3 mL of hexafluoroethane (C_2F_6, product of Messer MG Industries, PA) and 8.7 mL air were captured in the syringe, forming coarse foam with large bubbles. These large bubbles were broken into much smaller bubbles (mean volume-surface radius, R_{32}, in the range between 35 and 125 μm), by using a series of consecutive ejections and injections of the foam through the needle. Hexafluoroethane was used in the foam generation to reduce the rate of foam coarsening [28], during the rheological measurements, as a result of gas diffusion from the small toward the large bubbles (Ostwald ripening). The foam volume was measured at the end of the foam generation process to confirm that no extra air was trapped and the actual volume fraction of the bubbles corresponded to the required one. As an additional control, Φ was verified gravimetrically for several of the samples and no deviation larger than 1% was detected.

The bubble size distribution in the foams was determined immediately after finishing the rheological measurements, by using a procedure developed by Garrett et al. [60] and Mukherjee and Wiedersich [61]. In this method, about 1 mL of the foam is spread as a thick layer on the base-wall of a triangular prism. Images of the wetting films, formed in the zone of contact of the foam with the prism wall, are taken by video-camera, equipped with a long-focus magnifying lens (Micro Nikkor 55 mm). The illumination is accomplished by diffuse white light through one of the side-walls of the prism, whereas the observation is made through the other side-wall, under the condition of total internal reflection. Afterwards, the images are processed by Scion Image Analysis software to determine the areas, occupied by the individual bubbles on the wall surface. Finally, the distribution of the areas, occupied by the bubbles, is transformed into bubble-size distribution and the mean volume-surface radius, R_{32}, is determined. For more detailed description of the method, see Refs. [60,61].

3.1.3. Measurement of foam–wall friction stress

To measure the friction stress between a plug of foam and a smooth solid wall we used an ARES strain-controlled shear rheometer (Rheometrics Scientific), equipped with two parallel circular plates with radius, $R_P = 2.5$ cm. Glass circular plate was glued on the lower plate, whereas sandpaper of type 100 CG-Grade P was glued onto the upper plate – see Fig. 7A. The glass and sandpaper surfaces were optically examined to be parallel, with a deviation not exceeding ca. 0.1 mm in the entire area of the plates.

Before starting each experiment, the foam was loaded from the syringe used for foam generation, at relatively large gap between the plates (≈2 cm). Afterwards, the gap was reduced to the desired height (2 mm in most experiments; 1.5, 2.5 and 3 mm in some control experiments), the excess of foam was carefully removed by a spatula, and the lower plate was set in rotational motion, while the torque exerted on the upper plate, M, was measured by the rheometer sensor. In all experiments, the angular velocity of the lower plate, ω_R, was kept below the shear limit of the foam, so that the relative motion and, hence, the viscous friction were localized only in the region between the immobile plug of foam and the rotating lower glass plate. Before starting the actual measurements, several pre-runs were performed, which covered the entire range of velocities used in the actual measurement. During the rheological measurements, the parallel plates, and the foam intervening between them, were closed in a box to reduce water evaporation, which could induce foam destruction.

A given angular velocity of the circular plate corresponds to varying linear velocity of the plate surface, V_0, depending

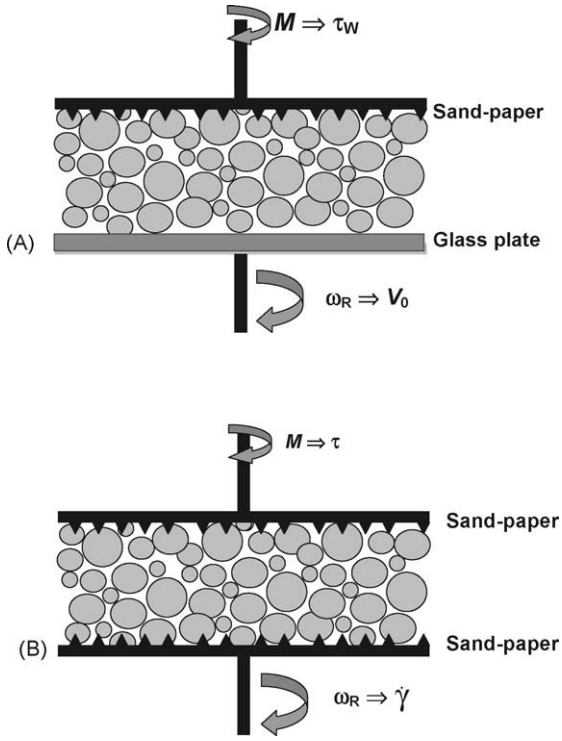

Fig. 7. Parallel-plates geometry used in the experiments for measuring: (A) foam–wall viscous stress; (B) viscous stress in sheared foam. The lower plate is rotated with angular velocity, ω_R, and the torque on the upper plate, M, is measured.

on the radial distance from the plate center, r:

$$V_0(r) = \omega_R r \tag{3.2}$$

Thus, at given ω_R, the measured torque is created by a friction, corresponding to different linear velocities of the plate with respect to the foam

$$M = \int_0^{R_P} 2\pi r^2 \tau[V_0(r)]\,dr \tag{3.3}$$

Assuming that the friction obeys a power law (see Eqs. (2.42) and (2.46))

$$\tau = \tau_W = k_W[V_0(r)]^m \tag{3.4}$$

one can integrate the local stress on the wall to obtain the total torque, M, which is the experimentally accessible quantity

$$M = 2\pi \frac{R_P^{m+3}}{(3+m)} k_W(\omega_R)^m \tag{3.5}$$

As seen from Eq. (3.5), the logarithm of the torque, $\ln M$, should be a linear function of $\ln\omega$. All results reported in this study are obtained by taking the linear portions of the respective experimental curves, to be sure that the data are described by a single power law function, with given m. From the slope of the linear fit to the data, we determined the power index, m, and from the intercept — the multiplier, k_W. Once m and k_W are determined, we plot the dependence of the wall stress, τ_W, on the linear velocity, V_0 (see Eq. (3.4)), or of the dimensionless wall stress, $(\tau_W R_{32}/\sigma)$, on the capillary number, $Ca^* = \mu V_0/\sigma$.

3.1.4. Measurement of the viscous friction inside sheared foam

The experimental setup, depicted in Fig. 7B, was used to measure the viscous stress inside sheared foam. In these experiments we used two parallel circular plates of radius $R_P = 2.5$ cm, covered with sandpaper (100 CG-Grade P), which had a grain-size approximately equal to the diameter of the bubbles in the studied foams. The shear rates were varied typically between 0.02 and 200 s^{-1} for mobile surfaces, and between 0.02 and 100 s^{-1} for immobile surfaces. Before starting the measurements with a given sample, several pre-runs were always performed, under the same conditions as those used in the actual rheological experiment. The measurement time was typically 6 s per point (measured after a 3 s pre-shear before the torque measurement at each shear rate). Direct experimental check showed that the results remained the same upon increase of this time by 50%. To be sure that the results are not affected by artefacts, caused by changes in the bubble size during the rheological measurement (due to foam coarsening or bubble breakup), only results obtained in two consecutive runs, spanning the entire range of shear rates and coinciding with each other, are presented. The bubble size was measured as explained in Section 3.1.2, immediately after finishing the rheological measurement with the given foam sample.

The gap width between the parallel plates, d_P, was 3 mm in most of the experiments. Control experiments at $d_P = 1.5$, 2, and 2.5 mm showed that the measured viscous stress in the foam was virtually independent of the used gap. The experimental results did not depend on the gap width, d_P, which evidenced that the wall-slip was negligible in these series of experiments, due to the appropriate choice of the sandpaper.

To account for the presence of elastic stress inside the sheared foam, we assumed that the foam obeys the rheological law of a Hershel-Bulkly (HB) fluid. Introducing Eq. (1.2) into Eq. (3.3), and taking into account that the local shear rate in the foam is $\dot\gamma(r) = V_0(r)/d_P = \omega_R r/d_P$, one obtains the following expression for the measured torque

$$M = \frac{2\pi R_P^3}{3}\left[\tau_0 + \frac{3}{(3+n)}\left(\frac{R_P}{d_P}\right)^n k_V(\omega_R)^n\right] \tag{3.6}$$

The fit of the experimental data with Eq. (3.6) allows one to determine the rheological parameters of the sheared foam, τ_0, n, and k_V. Since we are interested in this study by the viscous dissipation inside the foam, after determining the value of τ_0, the contribution of the elastic stress was excluded from the measured torque, and the experimental results were plotted as $\ln(\tau_V)$ versus $\ln(\dot\gamma)$, or as $\ln(\tau_V R_{32}/\sigma)$ versus the capillary number, $Ca = (\mu\dot\gamma R_{32}/\sigma)$, which gave straight lines with slope corresponding to the value of n.

3.2. Used materials

The following surfactants were used, as received from their producers: sodium dodecyl sulfate (SDS, product of Acros Organix, NJ); sodium dodecyl polyoxyethylene-3 sulfate (SDP3S; Steol CS-330 by Stepan, IL); cocoamidopropyl betaine (Tego Betaine F50; Goldschmidt Chemical, VA); sodium laurate (Na laur; TCI, Tokyo, Japan); potassium cocoylglycinate (K CocGlyc; Ajinomoto, Japan). In some of the experiments, 0.3 mM lauryl alcohol (LaOH; Sigma–Aldrich) was introduced as additive to SDS solutions to increase their surface modulus. Solutions of potassium myristate (K myr) and potassium palmytate (K palm) were prepared by dissolving myristic acid (Uniqema, New Castle, DE) and palmytic acid (Research Organics Inc., Cleveland, OH) in KOH solutions at 60 °C. Commercial facial cleanser, based on potassium soaps and diluted 10 times by deionized water before foam generation, was also included in the series of studied solutions, because it showed very high surface dilatational modulus (≈410 mN/m). Since K myr, K palm, and the commercial soap were only partly soluble in water, their solutions were thermostated for several hours and, just before foam preparation or measuring their surface dilatational modulus, they were filtered through 220 nm Millipore filters. In several series of experiments, glycerol (Acros, NJ) was added to the surfactant solutions to increase their viscosity. All solutions were prepared with deionized water from Millipore Organex water purification system.

3.3. Experimental results and discussion

3.3.1. Wall friction

The results from the measurements of the wall friction, with the various surfactant solutions studied, are summarized in Fig. 8 and Table 2. All results are obtained at air volume fraction of $\Phi = 90 \pm 1\%$.

As one can see from Table 2, the results for all systems fall into two groups: (1) surfactants with high surface modulus, $E_S > 100$ mN/m, which exhibit power law index $m = 1/2 \pm 5\%$; (2) Surfactants with low and moderate surface modulus, $E_S < 60$ mN/m, which show a power law index for the foam–wall friction, $m = 2/3 \pm 5\%$. Fig. 8A illustrates the difference between these groups with two of the surfactant solutions studied. The solution of the K soaps (K laur + K myr + K palm) has high surface modulus, $E_S = 210$ mN/m, and the slope in the dependence τ_W versus V_0 corresponds to $m = 1/2$. In contrast, Na laurate solution has $E_S = 1.5$ mN/m and, respectively, $m = 2/3$.

Fig. 8B summarizes the data for a series of Na laurate and K Cocoylglycinate solutions, containing glycerol of various concentrations (0–60 wt.%), used to modify the solution viscosity. All these solutions had surface modulus, $E_S < 60$ mN/m, and power index $m = 2/3$. As expected, the solutions with higher viscosity (higher glycerol concentration) showed higher viscous stress.

The same data, along with the results from experiments with several other surfactants, are represented in Fig. 8C as dimensionless stress, $\tau_W R_{32}/\sigma$, versus the capillary number, Ca^*. As seen from Fig. 8C, the results for solutions having high surface modulus (K soaps) merge into a master line with slope 1/2, whereas the results for the solutions with low surface modulus (Na laurate, Betaine, and K Cocoylglycinate) converge to another line with slope 2/3, despite the different viscosities of the solutions and different mean bubble radii in the various samples. Therefore, the scaling of the experimental data gives two master lines for tangentially immobile and for tangentially mobile bubble surface, respectively. Fig. 8C confirms the assumption that the theoretical friction laws, Eqs. (2.42) and (2.46), are independent of the specific chemical composition of the solution — only the surface mobility of the bubbles is important for switching between the two regimes with $m = 1/2$ and $m = 2/3$, respectively, if the surfactant solutions behave as Newtonian liquids (like those used in the current study).

One sees from Fig. 8C that the surfactants with tangentially immobile surface, $m = 1/2$, show higher viscous stress, at equivalent all other conditions. The latter result is anticipated, because the viscous friction occurs in the entire area of the wetting films in these systems, as explained in Section 2.6. From the comparison of Eqs. (2.42) and (2.46), with the ex-

Table 2
Results for the surface tension, σ, surface dilatational modulus, E_S, and power law index of foam–wall viscous friction, m

Surfactant	Surface tension, σ (mN/m)	Surface modulus E_S (mN/m)	Power law index, m
15 mM SDS	38.5	3	2/3 (±5%)
15 mM SDS + 0.3 mM LaOH	33.6	5	
36 mM SDS + betaine (1:1)	27.6	1	
3 wt.% betaine	28.4	<3	
3 wt.% SLES + 40 wt.% glycerol	30.6	<1	
1 wt.% Na laurate	29.3	1.5	
2 wt.% K cocoylglycinate	30.0	56	
1 wt.% K myristate	31.8	120	1/2 (±5.%)
0.25 wt.% K laurate + 0.5 wt.% K myristate + 0.25 wt.% K palmytate	27.3	210	
Commercial K soap	22.8	410	

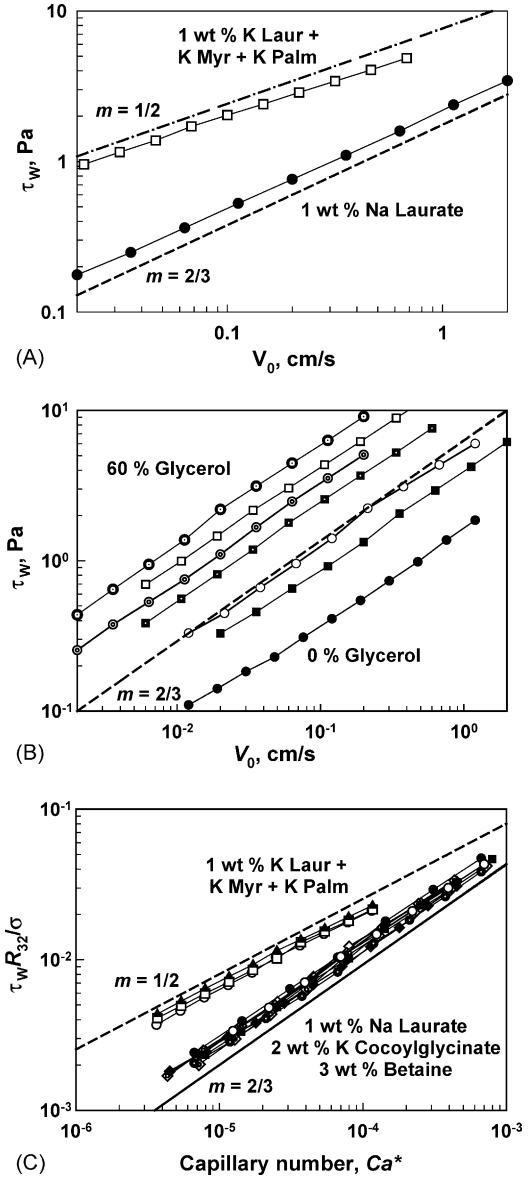

Fig. 8. Experimental results for the foam–wall viscous friction. (A) The points show experimental results for the wall stress, $\tau_W(V_0)$, whereas the dashed and the dot-dashed lines are drawn with slopes 2/3 and 1/2, respectively. (B) Results for $\tau_W(V_0)$, obtained with solutions of Na laurate (circles) and K Cocoylglycinate (squares), containing glycerol of various concentrations. (C) Dimensionless wall stress, $\tau_W R_{32}/\sigma$, vs. the capillary number, $Ca^* = \mu V_0/\sigma$, for various surfactant solutions (some of them containing glycerol).

perimental data shown in Fig. 8, one can determine the values of the numerical constants, $C_{IM} \approx 4.6$ and $C_M \approx 3.9$. These values of the constants indicate that the mean viscous stress, $\langle \tau_W \rangle$ in the wetting films of the 3D-foams is about 4 times higher than the mean stress in a wetting film, of the same radius, R_F, formed by a 2D-bubble (at the same all remaining parameters). This result indicates also that the wetting films in the case of a 3D-foam are probably 4 times thinner than the respective film for a 2D-bubble.

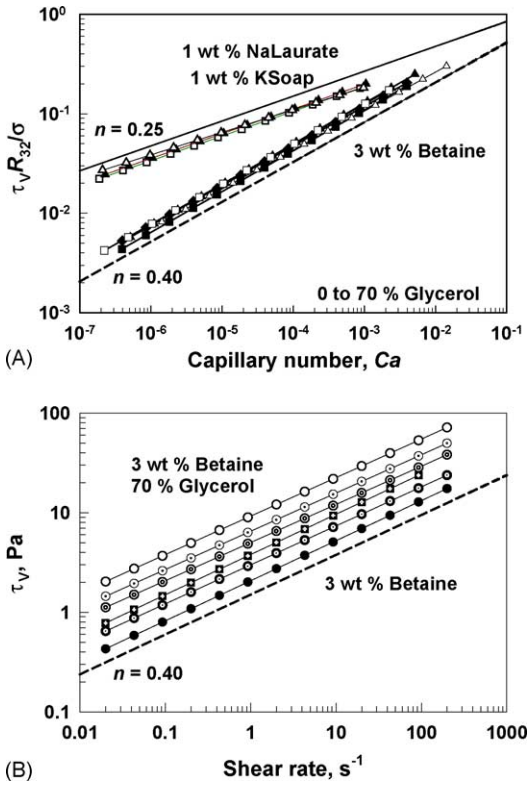

Fig. 9. Experimental results for the viscous friction inside continuously sheared foams. (A) The points represent experimental data for the dimensionless viscous stress, $\tau_V R_{32}/\sigma$, versus the capillary number, $Ca = \mu\dot{\gamma}R_{32}/\sigma$, whereas the two straight lines are drawn with slopes 0.25 and 0.40, respectively. (B) Results for $\tau_V(\dot{\gamma})$, obtained with Betaine solutions, containing glycerol of various concentrations.

3.3.2. *Viscous friction inside sheared foam*

The results from the measurements of the viscous stress, τ_V, inside sheared foams of volume fraction, $\Phi = 90 \pm 1\%$, are summarized in Fig. 9 and Table 3. The surfactant solutions, used to complete Table 3, contained 30 wt.% glycerol to increase their viscosity and, thus, to improve the accuracy of measuring τ_V. Again two different groups of surfactants are clearly distinguished. Those with low surface dilatational modulus exhibit a power law index, $n = 0.42 \pm 0.02$. The systems with high surface modulus, $E_S > 60$ mN/m, exhibit a power law index, $n = 0.24 \pm 0.02$.

The only exception from the observed general trends, in the studied systems, is the solution of 1 wt.% Na laurate, which shows relatively low surface dilatational modulus, $E_S = 4.5 \pm 0.5$ mN/m, while the respective power law index $n = 0.25 \pm 0.01$ (measured both in the absence and in the presence of 30 wt.% glycerol), is similar to those observed with tangentially immobile surfaces. In other words, this solution behaves as having tangentially immobile surfaces with respect to the friction inside the foam (Table 3), whereas it behaves as having tangentially mobile surfaces in the foam–wall friction (cf. Table 2). Such an apparent 'discrepancy' could be explained, taking into account the fact that the viscous dissipation occurs at two rather different characteristic time-

Table 3
Experimental results for the surface tension, σ, surface dilatational modulus, E_S, and power law index of viscous friction inside continuously sheared foam, n

Surfactant + 30 wt.% glycerol	σ (mN/m)	E_S (mN/m)	Power law index, n
7 mM SDS	36.2	4	0.41
10 mM SDS + 0.2 mM LaOH	31.5	6	0.42
1 wt.% SDS + 1 wt.% betaine	25.2	2	0.44
3 wt.% betaine	26.2	<3	0.40
2 wt.% SLES	31.2	<1	0.41
1 wt.% Na laurate	26.3	4.5	0.25
2 wt.% K cocoylglycinate	27.4	90	0.22
0.5 wt.% K laurate + 1 wt.% K myristate + 0.5 wt.% K palmytate	27.1	210	0.27
Commercial K soap	23.9	410	0.25

scales in the cases of foam–wall and 'inside-foam' friction. Inside sheared foam, the bubbles collide with each other at a characteristic frequency of the order of the shear rate, $\dot{\gamma}$, which varies between 0.02 and 200 s^{-1} in our experiments. In contrast, the foam–wall friction occurs at a quasi-steady state configuration of the bubbles, which corresponds to the zero-frequency limit of the surface oscillations. In our oscillating-drop experiments (Section 3.1.1), we were able to measure E_S at relatively low frequency, 0.125 s^{-1}. Therefore, the data for E_S are representative for the low-frequency regime of surface oscillations, and from this viewpoint, are more appropriate for comparison with the foam–wall friction. To make a proper comparison of the values of E_S with the results for the viscous stress inside sheared foams, measurements of E_S at higher frequencies are needed, which are impossible with the equipment available. In other words, we expect that E_S of 1 wt.% Na laurate solution rapidly increases with the frequency of oscillations and ensures tangentially immobile surfaces during the bubble-bubble collisions in sheared foams. This hypothesis will be checked in future experiments.

As seen from Fig. 9A and B, the scaling of the viscous stress and shear rate converges the results from different surfactant solutions, with various viscosities (between 1 and 15 m Pa s), into two master lines. Again, the solutions with tangentially immobile bubble surface exhibit higher viscous stress, at equivalent other conditions.

Additional experiments, performed at different volume fractions of air in the foam (Φ varied between 87 and 95 vol.%), showed that the power index for Betaine was virtually independent of Φ, $n \approx 0.40 \pm 0.02$. For the solution of commercial K soap, which exhibited high surface modulus and tangentially immobile surface, n noticeably decreased with the increase of Φ: from $n = 0.28 \pm 0.02$ at $\Phi = 0.87$, down to 0.17 ± 0.02 at $\Phi = 0.97$. As expected, the friction force always increased with the volume fraction of air in the foam, at equivalent all remaining conditions.

The comparison of the results, presented in Tables 2 and 3, shows that the power law indexes for foam–wall friction, m, and for the viscous friction inside sheared foam, n, are rather different from each other. The values of m can be explained theoretically by the models discussed in Section 2.6, whereas the measured values of n have no theoretical explanation, so far. It is worthwhile noting also that the values of n, measured in the current study with foams, are systematically lower than the values measured by Princen [5,6], $n \approx 0.5$, with emulsions having comparable volume fraction of the dispersed phase. The reasons for the different values of n for foams and emulsions are unclear at the present moment, and further studies are required to understand better the viscous friction inside these systems.

4. Conclusions

A theoretical model for the foam–wall friction is developed for tangentially immobile bubble surfaces. The model predicts that, at negligible contribution of the surface forces in the wetting film (which is typically the case for foams), the viscous wall stress, $\tau_W \propto (Ca^*)^{1/2}$, where the capillary number $Ca^* = (\mu V_0/\sigma)$ is defined with respect to the relative velocity of the foam and the solid wall, V_0. This result differs from the result of the Bretherton's model [24], which predicts $\tau_W \propto (Ca^*)^{2/3}$. The reasons for this difference are explained by considering the surface mobility of the bubbles.

The relevance of these two theoretical models, to real systems, is verified by measurements of the foam–wall friction for foams, generated from solutions with different surface properties (characterized by the oscillating drop method). The model, developed in the current study for tangentially immobile surfaces, could be useful for description of other systems of practical interest, e.g., bubbles and drops moving in capillaries [7,24,37–42,56,57].

Experiments with sheared foams demonstrated that the viscous friction inside the foam also depends strongly on the surface mobility of the bubbles. The foam stress was described very well by the Herschel–Bulkley model with power law index $n = 0.24 \pm 0.02$ for tangentially immobile and 0.42 ± 0.02 for tangentially mobile bubble surfaces, respectively, at air volume fraction $\Phi = 0.90$. The latter results still lack theoretical description.

Acknowledgments

The authors are grateful to Dr. H. Princen, Prof. H. Stone (Harvard University), and Dr. K.P. Ananth (Unilever R&D, NJ) for the useful and stimulating discussions. Mr. P. Singh and Mr. C. Ho (Unilever R&D, NJ) are acknowledged for

their valuable help in performing the experiments. The critical reading of the manuscript and the help in its preparation by Dr. S. Tcholakova (Sofia University) is gratefully appreciated.

References

[1] H.M. Princen, J. Colloid Interface Sci. 71 (1979) 55.
[2] H.M. Princen, J. Colloid Interface Sci. 105 (1985) 150.
[3] H.M. Princen, Langmuir 2 (1986) 519.
[4] H.M. Princen, A.D. Kiss, Langmuir 3 (1987) 36.
[5] H.M. Princen, A.D. Kiss, J. Colloid Interface Sci. 128 (1989) 176.
[6] H.M. Princen, in: J. Sjöblom (Ed.), Encyclopedia of Emulsion Technology, Marcel Dekker, New York, 2001, p. 243 (Chapter 11).
[7] A.M. Kraynik, Ann. Rev. Fluid Mech. 20 (1988) 325.
[8] A.M. Kraynik, M.K. Neilsen, D.A. Reinelt, W.E. Warren, in: J.F. Sadoc, N. Rivier (Eds.), Foams and Emulsions, Kluwer Academic Publishers, Netherlands, 1999, p. 259.
[9] A.M. Kraynik, D.A. Reinelt, J. Colloid Interface Sci. 181 (1996) 511.
[10] A.M. Kraynik, D.A. Reinelt, H.M. Princen, J. Rheol. 35 (1991) 1235.
[11] D.A. Reinelt, A.M. Kraynik, J. Colloid Interface Sci. 132 (1989) 491.
[12] S.A. Khan, C.A. Schnepper, R.C. Armstrong, J. Rheol. 32 (1988) 69.
[13] S.A. Khan, R.C. Armstrong, J. Rheol. 33 (1989) 881.
[14] A.J. Liu, S. Ramaswamy, T.G. Mason, H. Gang, D.A. Weitz, Phys. Rev. Lett. 76 (1996) 3017.
[15] T.G. Mason, J. Bibette, D.A. Weitz, J. Colloid Interface Sci. 179 (1996) 439.
[16] D.J. Durian, Phys. Rev. E 55 (1997) 1739.
[17] S. Cohen-Addad, H. Hoballah, R. Höhler, Phys. Rev. E 57 (1998) 6897.
[18] S. Cohen-Addad, R. Höhler, Y. Khidas, Phys. Rev. Lett. 93 (2004) 028302-1.
[19] M.E. Cates, P. Sollich, J. Rheol. 48 (2004) 193.
[20] D.M.A. Buzza, C-Y.D. Lu, M.E. Cates, J. Phys. II 5 (1995) 37.
[21] D.A. Edwards, D.T. Wasan, in: R.K. Prud'homme, S.A. Khan (Eds.), Foams: Theory, Measurements and Applications, Dekker, New York, 1996.
[22] D.A. Edwards, H. Brenner, D.T. Wasan, Interfacial Transport Processes and Rheology, Butterworth-Heinemann, Boston, 1991.
[23] L.W. Schwartz, H.M. Princen, J. Colloid Interface Sci. 118 (1987) 201.
[24] F.P. Bretherton, J. Fluid Mech. 10 (1961) 166.
[25] M. Duran, L. Jack, H.A. Stone, Presentation at the 5th Eurofoam Conference on Foams, Emulsions and Applications, Champs-sur-Marne, France, 5–8 July, 2004.
[26] H.A. Stone, S.A. Koehler, S. Hilgenfeldt, M. Durand, J. Phys.: Condens. Matter 15 (2003) 283.
[27] S.A. Koehler, H.A. Stone, M.P. Brenner, J. Eggers, Phys. Rev. E 58 (1998) 2097.
[28] S.A. Koehler, S. Hilgenfeldt, H.A. Stone, Langmuir 16 (2000) 6327.
[29] S.A. Koehler, S. Hilgenfeldt, E.R. Weeks, H.A. Stone, Phys. Rev. E 66 (2002) 040601-1.
[30] M. Durand, G. Martinoty, D. Langevin, Phys. Rev. E 60 (1999) 6307.
[31] M. Durand, D. Langevin, Eur. Phys. J. E7 (2002) 35.
[32] A. Saint-Jalmes, Y. Zhang, D. Langevin, Presentation at the 5th Eurofoam Conference on Foams, Emulsions and Applications, Champs-sur-Marne, France, 5–8 July, 2004.
[33] O. Pitois, C. Fritz, M. Vignes-Adler, J. Colloid Interface Sci. 282 (2005) 458.
[34] B. Herzhaft, J. Colloid Interface Sci. 247 (2002) 412.
[35] A. Yoshimura, R.K. Prud'homme, J. Rheol. 32 (1988) 53.
[36] M. Mooney, J. Rheol. 2 (1931) 210.
[37] G.J. Hirasaki, J.B. Lawson, Soc. Petrol. Eng. J. 25 (1985) 176.
[38] L.W. Schwartz, H.M. Princen, A.D. Kiss, J. Fluid Mech. 172 (1986) 259.
[39] K.G. Kornev, A.V. Neimark, A.N. Rozhkov, Adv. Colloid Interface Sci. 82 (1999) 127.
[40] I. Cantat, N. Kern, R. Delannay, Europhys. Lett. 65 (2004) 726.
[41] R. Delannay, I. Cantat, J. Etrillard, Presentation at the 5th Eurofoam Conference on Foams, Emulsions and Applications, Champs-sur-Marne, France, 5–8 July, 2004.
[42] J. Ratulowski, H.C. Chang, J. Fluid Mech. 210 (1990) 303.
[43] D. Dowson, G.R. Higginson, Elasto-hydrodynamic lubrication, in: The Fundamentals of Roller and Gear Lubrication, Pergamon Press, Oxford, 1966.
[44] B.N.J. Persson, Sliding Friction: Physical Principles and Applications, Springer, Berlin, 1998, p. 98 (Chapter 7).
[45] B.V. Derjaguin, N.V. Churaev, V.M. Muller, Surface Forces, Plenum Press, New York, 1987.
[46] J.N. Israelachvili, Intermolecular and Surface Forces, 2nd ed., Academic Press, New York, 1992.
[47] P.A. Kralchevsky, K.D. Danov, N.D. Denkov, in: K.S. Birdi (Ed.), Handbook of Surface and Colloid Chemistry, Second expanded and updated edition, CRC Press LLS, New York, 2002 (Chapter 5).
[48] A.D. Roberts, D. Tabor, Proc. R. Soc. Lond. A 325 (1971) 323.
[49] I.B. Ivanov, D.S. Dimitrov, Thin film drainage, in: I.B. Ivanov (Ed.), Thin Liquid Films: Fundamentals and Applications, Marcel Dekker, New York, 1988 (Chapter 7).
[50] V.G. Levich, Physicochemical Hydrodynamics, Prentice Hall, Englewood Cliffs, New Jersey, 1962.
[51] N.D. Denkov, A. Lips, in preparation.
[52] S.P. Meeker, R.T. Bonnecaze, M. Cloitre, Phys. Rev. Lett. 92 (2004) 198302-1.
[53] U. Seifert, Phys. Rev. Lett. 83 (1999) 876.
[54] P. Glansdorff, I. Prigogine, Thermodynamic Theory of Structure, Stability and Fluctuations, Wiley-Interscience, London, 1971.
[55] H.C. Cheng, R. Lemlich, Ind. Eng. Chem. Fundam. 22 (1983) 105.
[56] F. Fairbrother, A.E. Stubbs, J. Chem. Soc. 1 (1935) 527.
[57] G.I. Taylor, J. Fluid Mech. 10 (1961) 161.
[58] J. Lucassen, M. van den Tempel, Chem. Eng. Sci. 27 (1972) 1283.
[59] J. Lucassen, M. van den Tempel, J. Colloid Interface Sci. 41 (1972) 491.
[60] P.R. Garret, J.D. Hines, S.C. Joyce, P.T. Whittal, Report prepared for Unilever R&D, Port Sunlight, 1993.
[61] S. Mukherjee, H. Wiedersich, Colloids Surf. 95 (1995) 159.